Author/s:
Pearson, J;Nguyen, TL;Cölfen, H;Mulvaney, P

Title:
Sedimentation of C60 and C70: Testing the Limits of Stokes' Law

Date:
2018-11-01

Citation:
Pearson, J., Nguyen, T. L., Cölfen, H. & Mulvaney, P. (2018). Sedimentation of C60 and C70: Testing the Limits of Stokes' Law. Journal of Physical Chemistry Letters, 9 (21), pp.6345-6349. https://doi.org/10.1021/acs.jpclett.8b02703.

Sedimentation of C_{60} and C_{70} –Testing the Limits of Stokes' Law

Joseph Pearson [1], Tich Lam Nguyen [2], Helmut Cölfen [1], Paul Mulvaney [2]

[1] Physical Chemistry, Chemistry Department, University of Konstanz, Germany,

[2] ARC Centre of Excellence in Exciton Science, School of Chemistry, University of Melbourne, Parkville, VIC., 23010, Australia.

Abstract

Virtually all dynamic methods for determining particle size at the nanoscale use the Stokes-Einstein-Sutherland equation (SES) to convert the diffusion coefficient into a hydrodynamic radius. The validity of this equation at the nanoscale has not been rigorously validated by experiment. Here we measure the sedimentation rates and diffusion coefficients of C_{60} and C_{70} in toluene using analytical ultracentrifugation and compare the results to the SES equation. We find that the SES equation for the drag force (non-slip boundary condition) works down to 1 nm lengthscales.

Table of Contents Graphic

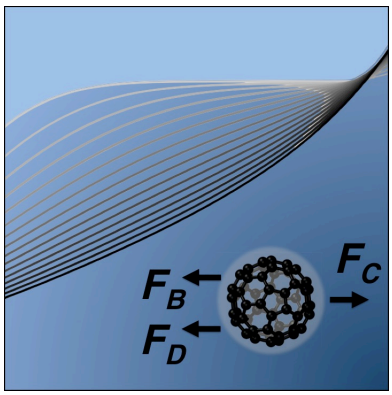

The determination of nanoscale particle sizes is an important challenge for the whole of chemistry. A plethora of materials have dimensions in this size regime including semiconductor nanocrystals, metal nanoparticles, polymers, micelles, microemulsions, vesicles, proteins, viruses, clay sheets as well as a host of carbon nanostructures such as nanotubes and graphene sheets. Sizing can be carried out by electron microscopy or atomic force microscopy but these involve sampling only a small fraction of the distribution and there is inherent observer bias[1]. Furthermore, during electron microscopy, many samples are damaged by exposure to the electron beam or to the high vacuum. The common alternative is to use an indirect approach such as dynamic light scattering (DLS) or analytical ultracentrifugation (AUC), which cede the diffusion coefficient of the objects and, in order to obtain the particle size, assume both a shape for the particles and the validity of the Stokes-Einstein-Sutherland equation[2-4]

$$D = \frac{kT}{6\pi a\eta(\mathrm{f}/\mathrm{f}_o)} \qquad [1]$$

Here a is the hydrodynamic radius, η is the solvent viscosity, k the Boltzmann constant, T solution temperature, and f/f_0 the frictional ratio, defined as the ratio of the particles' frictional coefficient to that of the equivalent sphere. i.e. the shape of equal volume but minimal surface area. Inherent in this equation is the assumption of non-slip boundary conditions at the surface. In general this equation is only valid for solutes significantly larger than the solvent molecules. Most particles in aqueous or non-aqueous solvents must be stabilized against aggregation by adsorbed surfactants, a hydration layer or adsorbed charges, resulting in a hydrodynamic size larger than that of the bare core. The volume and thickness of this layer is significant for particles less than 20 nm in size, which renders the determination of particle sizes complex, even when the sample is relatively monodisperse. The validity of the SES equation is also questionable once the particle radius approaches molecular dimensions. For very small molecular species with radii up to 3–5 Å, an empirical correction formula for the hydrodynamic radius from the SES equation was given by Schultz and Solomon based on viscometry data[5]. Several theoretical models predict a shift to slip boundary conditions for nanoscale solutes and to viscosity gradients near the surface, which may invalidate the SES equation [6-8]. The increased viscosity (typically 50 – 150 % higher compared to the bulk solution) and density of the surface solvation layer lead to increased hydrodynamic drag, which can be corrected for, leading to good agreement between experiment and a modified SES equation[8].

A further challenge is accounting for variations in nanoparticle shape. Extensive work on the molecular weight of proteins over several decades has led to the introduction of the shape factor, f/f_0, describing the relative asymmetry of the particles. This factor may account for both non-spherical geometry and the presence of solvation layers around the protein[9]. The solvation layer will include

bound solvent molecules and counter ions, which are necessary to maintain stability against aggregation. Values of f/f_0 ~1.2-1.4 are typically necessary to obtain agreement between theory and experiment[10].

It would be useful to confirm the validity of the SES equation down to nanometre or molecular dimensions. To achieve that, monodisperse probes are required with well-defined shape and density, which can be dispersed in a solvent without any coatings or stabilizers, yet without aggregation. A potential probe meeting these requirements is the fullerene family. C_{60} and C_{70} have well-defined crystallographic size, shape and molecular weight, and spontaneously dissolve to millimolar concentrations in several organic solvents[11-12]. They also have well-defined optical extinction coefficients. They are close in structure, differing by only 10 atoms, and therefore likely to exhibit very similar hydrodynamic behavior. Surprisingly, the sedimentation behaviour of fullerenes has not been reported to date, although there have been studies of carbon nanotubes[13-14].

Here we report that C_{60} and perhaps C_{70} are useful probes not only for AUC calibration but also for validating the Stokes-Einstein-Sutherland equation down to the smallest size regime to date (1 nm). Validation is a pre-requisite for the application of this equation to the sizing of molecular objects. The large body of work utilizing C_{60} makes it a particularly useful subject for comparison to other analytical methods, and will be the primary focus of discussion here. Comparison of the C60 and C70 results is included as a useful illustration of the resolving power of the method.

Samples of C_{60} and C_{70} were dispersed in toluene. Sedimentation data were collected over 11 hours in a Beckman ultracentrifuge equipped with multiwavelength absorbance optics, operating at 55,000 rpm and 20° C[15]. The sedimentation data were monitored at 470 nm and the absorbance data were fitted to the Lamm equation using the 'continuous c(s) with invariant D' model in the software program SedFit[16]. The sedimentation coefficient distribution was fit over a grid range from 0 to 5 S, with 100 point resolution, and the diffusion coefficient was allowed to float. Time and radially invariant noise, as well as the positions of the meniscus and cell bottom were also fitted. A confidence level of 0.7 was applied. Typical results are shown in Figure 1, where the time and space dependent concentration of C_{60} measured from its absorbance at 470 nm are presented.

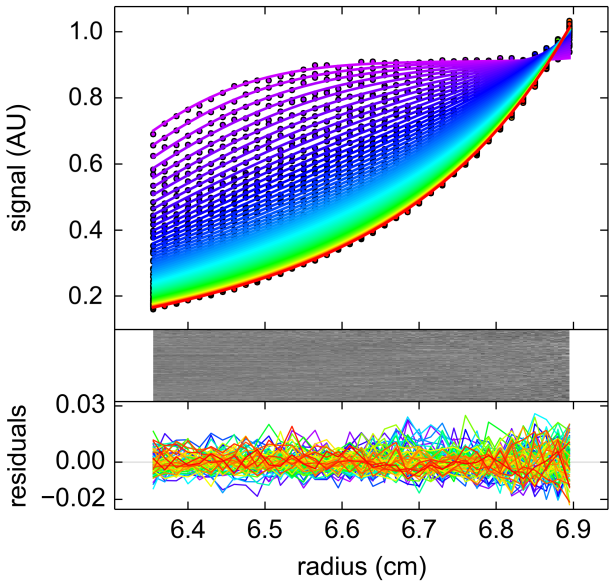

Figure 1: Top: Time and space dependent absorption profiles at 470nm during sedimentation of C_{60} in toluene at 55,000 rpm and 20° C. Time increases from the purple traces through to the red traces. The radial distances are measured from the rotor axis. The lines show the Lamm equation model fit to the experimental data points using SedFit. Note the long-term concentration profile is close to the exponential sedimentation equilibrium distribution expected as the sedimentation and diffusion fluxes approach equilibrium. Middle: Residuals as a 2D bitmap. Bottom: Residuals across radial scan traces, showing very little systematic error and RMSD = 0.006.

Numerical fitting using SedFit solves the inverse problem of identifying sedimentation and diffusion coefficients that give rise to the experimentally observed solute redistribution during centrifugation. The well-known Lamm equation is a partial differential equation describing the concentration flux due to diffusion and sedimentation with cylindrical divergence in a centrifugal field. No exact solutions to the Lamm equation exist, but may be approximated numerically[17-18]. The best model is derived from a sum of finite element solutions of the Lamm equation through least squares fitting. This recovers a concentration distribution of sedimentation coefficients, c(s), where distribution peaks may be integrated to yield weight average sedimentation coefficients. Importantly, fitting the sedimentation data yields two independent values: a weighted average diffusion coefficient and sedimentation coefficient. No prior knowledge about particle density, shape or solvent conditions is imposed in the fitting. The numerical fitting accounts for back diffusion from solute accumulating at the bottom of the cell, which is important for small S particles, where diffusion dominates the sedimentation profile. A c(s) plot for C_{60} is shown in Figure 2. We find that both C_{60} and C_{70} exhibit very clean sedimentation dynamics with no evidence for dimers or oligomers at larger S values. A small bump at <0.2 S is due to instrument noise or an error in the baseline fitting.

We firstly consider the diffusion coefficient value. To compare the C_{60} value of D obtained here to those found from other methods with different solvents requires conversion to standard conditions, $D_{20,w}$[19]. The conversion is made by multiplying the measured value of D by the ratio of solvent temperatures and the viscosity of the solvent used to that of water at 20° C, i.e. $D_{20,w} = D\left(\eta / \eta_w\right)\left(T_w / T\right)$.

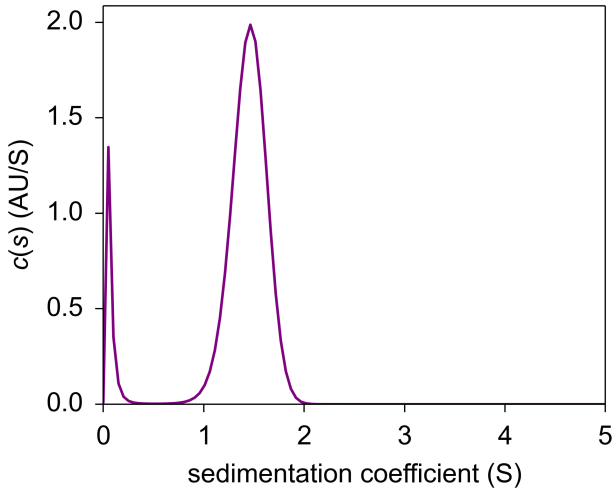

Figure 2: Sedimentation coefficient distribution, c(s) for C_{60} sedimented at 55,000 rpm and 20° C. The weight average sedimentation coefficients are 1.44 S for C_{60} and 1.47 S for C_{70}. The weight average diffusion coefficients are 7.591x10^{-6} cm^2/s for C_{60} and 7.335x10^{-6} cm^2/s for C_{70}.

Table 1 – Diffusion Coefficients of C_{60} and Calculated Radii (Å)

C60 D from literature method	D cm^2/s	T K	Solvent	viscosity mPa-s	$D_{20,w}$ cm^2/s	a_D Å	$a_{'slip'}$ Å	Ref.
AC Voltametry	1.70E-05	298.00	Dichloromethane	0.473	7.89E-06	2.71	4.07	21
Chronoamperometry	1.40E-05	298.15	Dichloromethane	0.473	6.50E-06	3.30	4.95	23
Chronoamperometry	1.05E-05	298.15	Dichloromethane	0.473	4.87E-06	4.40	6.60	24
RDE Voltammetry	1.40E-06	295.15	Benzonitrol	1.240	1.72E-06	12.45	18.68	20
AC Voltametry	2.60E-06	298.00	Benzonitrile	1.388	3.54E-06	6.05	9.07	21
Chronoamperometry	4.10E-06	298.15	Benzonitrile	1.388	5.58E-06	3.84	5.76	23
SS voltammetry	3.14E-06	295.15	Benzonitrile	1.240	3.86E-06	5.55	8.33	27
NMR pulsed gradient	8.30E-06	298.00	Benzene d6	0.641	5.22E-06	4.10	6.15	25
NMR pulsed gradient	1.85E-05	298.00	CS2	0.350	6.36E-06	3.37	5.06	22
NMR pulsed gradient	9.10E-06	298.00	C6H6	0.652	5.82E-06	3.68	5.52	22
Taylor dispersion	1.97E-07	297.65	Squalene	29.70	5.75E-06	3.73	5.59	26
Average						4.83	7.25	
AUC [This work]	7.59E-06	293.15	Toluene	0.585	4.43E-06	4.83	7.25	

Table 2 - Diameter of C_{60} determined by Physical Methods

Method	Radius, a (Å)	Ref.
NMR[a]	5.10	28
Gas Phase Electron Diffraction[b]	5.24	30
Single Crystal XRD at 110 K[b]	5.21	31
Powder XRD[b]	5.22	33
HRTEM	5.05	29
STM	4.75	32
Average	5.09	

a; The average diameter from C centers is measured, and the value of 1.675 Å is added to each side to account for the π electron cloud on the outer edges

b; The average diameter from C centers is measured, the value of 1.675 Å from Dresselhaus is added to each side to account for the π electron cloud on the outer edges

As evident from the data in Table 1, the diffusion coefficients, D, obtained from AUC closely match the mean of those obtained earlier using other, independent methods[20-27]. Our value is 5% smaller than the average van der Waals radius of 5.09 Å reported from a number of physical methods listed in Table 2[28-33]. Note that, because almost all of the methods in Table 1 use the SES equation to determine the size, the value alone does not confirm the validity of eq. [1].

Hence, we now examine the sedimentation coefficient, S, using eq. [2], formulated from the Svedberg equation with Stokes drag, $F_D=6\pi a\eta v$ (v = speed), substituted for the hydrodynamic drag force, F_D and assuming spherical geometry.

$$S = \frac{2a^2(\rho_{C_{60}} - \rho_{solv})}{9\eta} \qquad [2]$$

Equation [2] is derived from a mechanical force balance of the centrifugal force, F_C, buoyant force F_B, and drag force F_D, and allows for the diameter of the C_{60} molecule to be determined independently from the mean sedimentation speed, provided that the mass density of C_{60} is known. A wide range of density values have been reported for the C_{60} molecule, including values gleaned using densitometry[34-35]. Other literature values for density have been deduced from crystallographic size measurements[28, 34]. The density may be directly computed from the radius and the molecular weight of C_{60} (720.66 g/mol). Considering the average radius of C_{60} reported by various physical methods, 5.09 Å, a density of 2.17 g/cm^3 is retrieved. Inserting the C_{60} density estimate (2.17 g/cm^3) and solvent viscosity (η = 0.585 mPa s), into equation [2] we obtain a = 5.41 Å, which is 6.3% larger than the average, reported, van der Waals value.

Utilizing both S and D from AUC, uniquely specifies a particle density, according to eq. [3].

$$D = \frac{\sqrt{2}}{18\pi} k_B T s^{-1/2} \left(\eta\left(f / f_0\right)_w\right)^{-3/2} \left((1 - \bar{\upsilon}_p \rho_S) / \bar{\upsilon}_p\right)^{1/2} \qquad [3]$$

Equation [3] is derived by combining the Svedberg equation and the SES equation. The C_{60} density, 2.49 g/cm^3, determined by S and D from AUC, and with Equation [3], is 14.9% larger than the average density value implied by other physical methods, whereas the radius from AUC is only 5% smaller. Because the density computation has a cubic dependency on radius, small discrepancies in size result in large differences in interpretations of density. S and the implied particle density, or D, may be used to calculate the particle radius by equation [2], or equation [1], equivalently resulting in C_{60} a = 4.83 Å (For C_{70}, we obtain a = 5.01 Å). These values assume non-slip boundary conditions.

In summary, we find that the SES equation provides a consistent explanation for the observed sedimentation speed and the diffusion coefficient of C_{60}, which in turn supports the application of non-slip boundary conditions down to radii of 1 nm. The resolution possible with the AUC method is illustrated in the less than 4% difference identified between the sedimentation and diffusion coefficients of C60 and C70. Finally, we consider potential sources of error in this analysis. Solvents may compress in AUC resulting in a density and viscosity gradient across the sample channel. The effect is small for aqueous solutions and is generally ignored. SedFit allows for the modelling of solvent compressibility. The compressibility factor of toluene, 894 Pa^{-1}, was considered in the fitting; however it resulted in a change in S of <2%, that was not consistent between the two samples[36].

The possibility of solute non-ideality was also considered by examining subsets of the sedimentation scans. Sets of 50 scans from the early, middle and late parts of the experiment were analysed independently. No systematic error was observed between the sets of analysis, indicating the solute was stable throughout the experiment.

The extinction coefficient for C_{70} at 472 nm is 22,420 M^{-1}cm^{-1} in o-xylene, although it varies slightly with solvent[37]. This yields concentrations in our AUC experiments of ~1 μM. Hence interparticle hydrodynamic effects do not play a role in the sedimentation behaviour.

We briefly consider the effects of altering f/f_0. For C_{70}, a slight oblateness is predicted from crystallographic models and theoretical calculations, with the aspect ratio approaching 1.1 according to Dresselhaus [38]. For an ellipse with this aspect ratio, the f/f_0 value is 1.0008 and consequently very little effect is predicted on the S values. However C_{70} is likely denser than C_{60}, which would lead to a slightly higher sedimentation rate and slightly lower diffusion coefficient. Hence we believe the C_{70} sediments effectively as a sphere, probably because of its very fast rotational diffusion. In the case of C_{60}, if we relax the SES conditions and assume slip boundary conditions, with the Stokes drag being given by $F_D=4\pi a\eta v$, then we obtain a much larger fullerene radius of 7.25 Å, inconsistent with other

physical sizing methods. This would imply that a layer of bound solvent molecules is adsorbed to the fullerene during diffusion. However, a larger radius is incompatible with slip, since this is predicated on weaker, not stronger, solvent interactions with the surface. Hence we believe our S and D values strongly validate the use of non-slip boundary conditions. This suggests that even for molecules down to 1 nm in size, if the particle is well dispersed in the solvent, then it is likely that non-slip boundary conditions prevail. Furthermore, fullerenes provide an easily prepared probe for AUC calibration, which is highly reproducible and therefore constitutes an outstanding calibration standard for accurate and reproducible nanoscale sizing.

Acknowledgements: The authors thank Wallace Wong for the fullerene samples. PM thanks the ARC for support through centre grant CE170100026. HC and JP acknowledge support by Deutsche Forschungsgemeinschaft (SFB 1214, Project B6)

References:

1. Villarrubia, J. S.; Vladár, A.; Postek, M. T., Scanning Electron Microscope Dimensional Metrology Using a Model‐Based Library. *Surface and Interface Analysis: An International Journal devoted to the development and application of techniques for the analysis of surfaces, interfaces and thin films* **2005**, *37*, 951-958.
2. Einstein, A., Über Die Von Der Molekularkinetischen Theorie Der Wärme Geforderte Bewegung Von in Ruhenden Flüssigkeiten Suspendierten Teilchen. *Annalen der physik* **1905**, *322*, 549-560.
3. Stokes, G. G., *On the Effect of the Internal Friction of Fluids on the Motion of Pendulums*; Pitt Press Cambridge, 1851; Vol. 9.
4. Sutherland, W., Lxxv. A Dynamical Theory of Diffusion for Non-Electrolytes and the Molecular Mass of Albumin. *The London, Edinburgh, and Dublin Philosophical Magazine and Journal of Science* **1905**, *9*, 781-785.
5. Schultz, S. G.; Solomon, A., Determination of the Effective Hydrodynamic Radii of Small Molecules by Viscometry. *The Journal of general physiology* **1961**, *44*, 1189-1199.
6. Van Holde, K.; Kensal, D., *Physical Biochemistry*, 1971.
7. Mächtle, W.; Börger, L., *Analytical Ultracentrifugation of Polymers and Nanoparticles*; Springer Science & Business Media, 2006.
8. Zhang, X.; Tran, S.; Gray-Weale, A., Hydrodynamic Drag on Diffusing Nanoparticles for Size Determination. *The Journal of Physical Chemistry C* **2016**, *120*, 21888-21896.
9. Cohn, E. J.; Edsall, J. T., *Proteins, Amino Acids and Peptides as Ions and Dipolar Ions*; Reinhold Publishing Corporation; New York, 1943.
10. Walser, R.; Mark, A. E.; van Gunsteren, W. F., On the Validity of Stokes' Law at the Molecular Level. *Chem Phys Lett* **1999**, *303*, 583-586.
11. Marcus, Y.; Smith, A. L.; Korobov, M.; Mirakyan, A.; Avramenko, N.; Stukalin, E., Solubility of C60 Fullerene. *The Journal of Physical Chemistry B* **2001**, *105*, 2499-2506.
12. Ruoff, R.; Tse, D. S.; Malhotra, R.; Lorents, D. C., Solubility of Fullerene (C60) in a Variety of Solvents. *The Journal of Physical Chemistry* **1993**, *97*, 3379-3383.
13. Fagan, J. A.; Zheng, M.; Rastogi, V.; Simpson, J. R.; Khripin, C. Y.; Silvera Batista, C. A.; Hight Walker, A. R., Analyzing Surfactant Structures on Length and Chirality Resolved (6, 5) Single-Wall Carbon Nanotubes by Analytical Ultracentrifugation. *Acs Nano* **2013**, *7*, 3373-3387.

14. Walter, J.; Löhr, K.; Karabudak, E.; Reis, W.; Mikhael, J.; Peukert, W.; Wohlleben, W.; Cölfen, H., Multidimensional Analysis of Nanoparticles with Highly Disperse Properties Using Multiwavelength Analytical Ultracentrifugation. *Acs Nano* **2014**, *8*, 8871-8886.
15. Bhattacharyya, S. K.; Maciejewska, P.; Börger, L.; Stadler, M.; Gülsün, A. M.; Cicek, H. B.; Cölfen, H., Development of a Fast Fiber Based Uv-Vis Multiwavelength Detector for an Ultracentrifuge. In *Analytical Ultracentrifugation, Progress in Polymer and Colloid Science*, Springer: Berlin Heidelberg, 2006; Vol. VIII, pp 9-22.
16. Schuck, P. Sedfit. http://www.analyticalultracentrifugation.com/default.htm
17. Demeler, B.; Saber, H., Determination of Molecular Parameters by Fitting Sedimentation Data to Finite-Element Solutions of the Lamm Equation. *Biophys J* **1998**, *74*, 444-454.
18. Schuck, P., Size-Distribution Analysis of Macromolecules by Sedimentation Velocity Ultracentrifugation and Lamm Equation Modeling. *Biophys J* **2000**, *78*, 1606-1619.
19. Ikeuchi, H.; Fujita, Y.; Iwai, K.; Satô, G. P., Precise Measurement of Ionic Diffusion Coefficients with a Hanging Mercury Drop Electrode. *Bulletin of the Chemical Society of Japan* **1976**, *49*, 1883-1887.
20. Dubois, D.; Moninot, G.; Kutner, W.; Jones, M. T.; Kadish, K. M., Electroreduction of Buckminsterfullerene, C60, in Aprotic Solvents. Solvent, Supporting Electrolyte, and Temperature Effects. *The Journal of Physical Chemistry* **1992**, *96*, 7137-7145.
21. Fawcett, W. R.; Opallo, M.; Fedurco, M.; Lee, J. W., Kinetics and Thermodynamics of the Electroreduction of Buckminsterfullerene in Benzonitrile. *J Am Chem Soc* **1993**, *115*, 196-200.
22. Haselmeier, R.; Holz, M.; Kappes, M.; Michel, R.; Fuchs, D., Translational Diffusion in C60 and C70 Fullerene Solutions. *Berichte der Bunsengesellschaft für physikalische Chemie* **1994**, *98*, 878-881.
23. Hishida, Y.; Nishi, M.; Baba, Y.; Ikeuchi, H., Diffusion Coefficients of C60 and C60-in Benzonitrile and Dichloromethane Solutions Containing Tetrabutylammonium Perchlorate, Measured by Potential-Step Chronoamperometry. *Analytical sciences* **2006**, *22*, 931-935.
24. Jung, Y.-J.; Kwak, J.-Y., Simultaneous Determination of Diffusion Coefficient and Concentration by Chronoamperometry at a Microdisk Electrode. *Bulletin of the Korean Chemical Society* **1994**, *15*, 209-213.
25. Kato, T.; Kikuchi, K.; Achiba, Y., Measurement of the Self-Diffusion Coefficient of Fullerene C60 in Benzene-D6 Using Carbon-13 Pulsed-Gradient Spin Echo. *The Journal of Physical Chemistry* **1993**, *97*, 10251-10253.
26. Kowert, B. A.; Watson, M. B., Diffusion of Organic Solutes in Squalane. *The Journal of Physical Chemistry B* **2011**, *115*, 9687-9694.
27. Mirkin, M. V.; Bulhoes, L. O.; Bard, A. J., Determination of the Kinetic Parameters for the Electroreduction of Fullerene C60 by Scanning Electrochemical Microscopy and Fast Scan Cyclic Voltammetry. *J Am Chem Soc* **1993**, *115*, 201-204.
28. Dresselhaus, M. S.; Dresselhaus, G.; Eklund, P. C., *Science of Fullerenes and Carbon Nanotubes: Their Properties and Applications*; Elsevier, 1996.
29. Goel, A.; Howard, J. B.; Vander Sande, J. B., Size Analysis of Single Fullerene Molecules by Electron Microscopy. *Carbon* **2004**, *42*, 1907-1915.
30. Hedberg, K.; Hedberg, L.; Bethune, D. S.; Brown, C.; Dorn, H.; Johnson, R. D.; De Vries, M., Bond Lengths in Free Molecules of Buckminsterfullerene, C60, from Gas-Phase Electron Diffraction. *Science* **1991**, *254*, 410-412.
31. Liu, S.; Lu, Y.-J.; Kappes, M. M.; Ibers, J. A., The Structure of the C60 Molecule: X-Ray Crystal Structure Determination of a Twin at 110 K. *Science* **1991**, *254*, 408-410.
32. Murphy, B. The Physico-Chemical Properties of Fullerenes and Porphyrin Derivatives Deposited on Conducting Surfaces. Trinity College Dublin, 2014.
33. Stephens, P. W.; Mihaly, L.; Lee, P. L.; Whetten, R. L.; Huang, S.-M.; Kaner, R.; Deiderich, F.; Holczer, K., Structure of Single-Phase Superconducting K3c60. *Nature* **1991**, *351*, 632.

34. Krätschmer, W.; Lamb, L. D.; Fostiropoulos, K.; Huffman, D. R., Solid C60: A New Form of Carbon. *Nature* **1990**, *347*, 354.
35. Ruelle, P.; Farina-Cuendet, A.; Kesselring, U., Changes of Molar Volume from Solid to Liquid and Solution: The Particular Case of C60. *J Am Chem Soc* **1996**, *118*, 1777-1784.
36. Richard, A. J.; Rogers, K. S., The Isothermal Compressibility of Organic Liquids by Ultracentrifugation. Correlation with Surface Tension. *Canadian Journal of Chemistry* **1971**, *49*, 3956-3959.
37. Toerpe, A.; Belton, D. J., Improved Spectrophotometric Analysis of Fullerenes C60 and C70 in High-Solubility Organic Solvents. *Analytical Sciences* **2015**, *31*, 125-130.
38. Nikolaev, A. V.; Dennis, T. J. S.; Prassides, K.; Soper, A. K., Molecular Structure of the C70 Fullerene. *Chem Phys Lett* **1994**, *223*, 143-148.